

A Boundary Element Model of Multiple Microcirculatory Bubbles in Cardiovasculature

Navish Wadhwa^a, Vardhman Jain^b, J. Brian Fowlkes^c, Joseph L. Bull^d and Brijesh Eshpuniyani^e

^a National Centre for Biological Sciences, Bangalore 560065, India,

^b iRunway India Private Limited, Hosur Road, Bangalore 560068 India,

^c Department of Radiology, University of Michigan, Ann Arbor, MI 48109-2110, USA,

^d Department of Biomedical Engineering, University of Michigan, Ann Arbor, MI 48109-2110, USA,

^e Department of Aerospace Engineering, IIT Kanpur, UP 208016, India

ABSTRACT

In order to investigate the role of gravity in a novel cancer treatment strategy called Gas Embolotherapy, we have computationally studied the evolution dynamics of two bubbles sticking to and sliding on the opposite walls of a 2D channel, under gravity-driven flow. We have modeled the moving three-phase contact lines using Tanner laws including contact angle hysteresis and have accounted for the gas-liquid interfacial dynamics in our model. Our model uses a Boundary Element Method (BEM) based moving-interface, multi-domain, iterative method to compute the flows and stresses on the domain boundaries at various instants of time. Since the normal and shear stresses acting on the endothelial layer of blood vessels are a major concern in the development of gas embolotherapy, we have examined the effect of bubble evolution and induced flows on the wall stresses. For a range of initial bubble pressures, we have studied the role of gravity by varying the Bond number and by using two different inclinations of the channel (horizontal and vertical) with respect to gravity. Our results suggest that the strength of gravitational forces and the inclination of the channel have a pronounced effect on both the bubble evolution and the resulting wall stresses. Aside from gravitational effects, the interaction of the bubbles through the surrounding fluid has a significant effect on their evolution. We have also examined the flow rates at both ends of the channel resulting from the evolution of the two bubbles.

1. INTRODUCTION

The motivation behind the current work comes from a novel cancer treatment strategy called gas embolotherapy, which is currently under development [1, 2]. In gas embolotherapy, small droplets ($\sim 6 \mu\text{m}$) of DDFP (C_3F_{12} ; dodecafluoropentane), coated with a layer of saline and albumin, are introduced into the blood stream at a convenient location and tracked using regular ultrasound. DDFP has a boiling point of 29°C at atmospheric pressure and is thus superheated at body temperature. It is prevented from spontaneous vaporization by the shell of albumin. These droplets are selectively vaporized at the desired location by rupturing the albumin shell using a high intensity ultrasound (acoustic droplet vaporization or ADV, [3, 4, 5]). The bubbles of DDFP thus formed become lodged in the microvasculature in or around the tumor, occluding the blood flow to the tumor and thus causing necrosis.

Several experimental studies have been reported involving gas bubbles in close proximity of solid walls [6–12]. However, there have been few attempts to study confined gas bubbles sticking to the channel walls. Cavanagh and Eckmann experimentally studied the behavior of a gas bubble sticking to the wall of an inclined tube [6, 7]. They provided counter-flow to keep the bubble lodged inside the tube and studied the effects of inclination and addition of surfactants. Eshpuniyani, Fowlkes and Bull [13] studied bubble transport through a bench top experimental model of a bifurcating tubular network.

While such experimental studies provide important information regarding bubble transport, they tell us little about the nature of normal and shear stresses acting on the walls. Normal and shear stresses play a vital role in health of the blood vessels as the endothelium, the innermost layer of the blood vessels, is known to respond to mechanical stimuli in the blood [14]. Changes in the haemodynamic shear stresses can have a variety of effects on the endothelial cell layer including changes in morphology [15–17], cytoskeleton organization [18–20], ion channel activation [21–23] and expression of genes [24, 25]. Thus, high normal and shear stresses in the vasculature can potentially cause damage to the endothelium, which is a major area of concern in the development of embolotherapy [1, 2].

In order to intelligently design the treatment and to make it more effective, it is imperative to have detailed quantitative information regarding the wall stresses and evolutionary behavior of gas bubbles inside the microvasculature. Previous attempts in this direction have considered a rapidly growing bubble in the centre of a capillary [2, 26] and a single bubble sticking to and sliding along capillary walls with and without contact angle hysteresis [27, 28].

Ye and Bull [2, 26] computationally investigated the evolution of a single bubble placed in a channel without touching any of the walls, with the purpose of simulating the process of droplet vaporization during ADV and to study its effect in terms of wall stresses. Subsequently, Eshpuniyani et al [27, 28] modeled the evolution of a single bubble sticking to the wall and studied the associated wall stresses. They looked at the effect of contact angle hysteresis on the bubble behavior and were able to demonstrate “stick and slide” behavior of the bubble. But they considered only a pressure gradient to be causing a background flow in the system and did not include gravitational effects in their model. In a separate study, we have investigated the effect of gravity on the behavior of a single bubble sticking to and sliding along a 2D channel wall.

In embolotherapy, many droplets are introduced into the blood stream at once, leading to the formation of a large number of gas bubbles which become lodged very close to each other in the capillaries. While the studies mentioned above have looked at the flow occlusion and wall stresses caused by a single bubble inside microvasculature, none of them have considered the effect of the presence of multiple bubbles inside the microvasculature, their interaction with each other or the surrounding fluid flow.

In this paper, we present a simple model of multiple bubbles inside microvasculature. We have modeled the microvessel as a two-dimensional channel containing a Newtonian fluid. We have modeled the bubbles as movable interfaces with an initial semicircular configuration, sticking to two opposite walls of the channel. In our model, we have included the interfacial dynamics and motion of the bubble governed by contact line dynamics. We have studied the effects of variation of the relative strength of gravitational forces with respect to the surface tension forces. We have also considered the effect of different angles of inclination of the channel, covering a whole parametric range. Here we present some selected cases which help illustrate the roles of various factors in the evolution dynamics and wall stress effects of multiple bubbles inside microvasculature.

2. ASSUMPTIONS

The general problem of transport of a gas bubble through the microvasculature is complicated as it is governed by numerous factors such as gravity, flow rate, convective and unsteady inertia, surface tension and the non-Newtonian nature of blood [1, 2, 26–28]. Several assumptions have been made in order to simplify the model and make it computationally tractable. We have modeled the microvessel as a two-dimensional channel with rigid walls. Although the walls are flexible in the case of large vessels, in the case of microvessels this assumption becomes reasonable because microvessels are embedded deep inside organs and are therefore held rigid by the surrounding tissue. We have assumed blood to be an incompressible Newtonian fluid. This allows us to model our flow using the Stokes equation which can be solved with the boundary element method (BEM). At a later date, we will extend our BEM model to explicitly include the presence of red blood cells [29]. Further, the gas inside the bubble is assumed to be an ideal gas, and the expansion/contraction of the bubble is assumed to be isothermal in nature. The contact line (junction between solid, liquid and gaseous phases) velocity has been modeled using modified Tanner laws including contact angle hysteresis [27, 28, 30], according to which the contact line velocity is proportional to deviation of the dynamic contact angle from the advancing or receding contact angle. Details of Tanner laws are discussed in the Initial and Boundary Conditions section.

3. GOVERNING EQUATIONS

The governing equations for the conservation of mass and momentum in an incompressible Newtonian fluid are the well known Navier-Stokes equations, which can be suitably written in their non-dimensional form as-

$$\text{Continuity:} \quad \vec{\nabla} \cdot \vec{u} = 0 \quad (1)$$

$$\text{Momentum:} \quad Ca \cdot \text{Re} \left\{ \frac{\partial \vec{u}}{\partial t} + (\vec{u} \cdot \vec{\nabla}) \vec{u} \right\} = -\vec{\nabla} p + Bo \vec{e}_g + Ca \cdot \nabla^2 \vec{u} \quad (2)$$

Where \vec{u} and p are velocity and pressure respectively. Non-dimensionalization has been done using $L^* = \text{half channel width}$ as the reference length scale and $U^* = \gamma^* / \mu^*$ as the reference velocity scale where γ^* is the surface tension and μ^* is the dynamic viscosity, and $P^* = \gamma^* / L^*$ as the reference pressure scale. Here $Ca = \mu^* U^* / \gamma^*$ is the capillary number and $\text{Re} = U^* L^* \rho^* / \mu^*$ is the Reynolds number, where ρ^* is the density. The choice of reference velocity scale makes the value of capillary number equal to 1. Bo represents the Bond Number which is a measure of the ratio of gravitational forces to surface tension forces ($Bo = \rho^* g L^* / \gamma^*$). Since the focus of our present study concerns flows in microvasculature which are characterized by very low values of Reynolds number, inertia terms from Equation 2 can be dropped to obtain-

$$\text{Stokes Equation:} \quad -\vec{\nabla} p + Bo \vec{e}_g + Ca \cdot \nabla^2 \vec{u} = 0 \quad (3)$$

4. NUMERICAL METHOD

The solution of linear, elliptic, homogenous partial differential equations as obtained in our problem can be represented by boundary integrals that involve the unknown function and its derivatives. For two-dimensional Stokes flow-

$$c_{kj} u_k(\vec{x}_o) = \frac{-1}{4\pi Ca C} \int f_i(\vec{x}, \vec{x}_o) G_{ij}(\vec{x}, \vec{x}_o) dl(\vec{x}) + \int u_i(\vec{x}) T_{ijk}(\vec{x}, \vec{x}_o) n_k(\vec{x}) dl(\vec{x}) \quad (4)$$

where C is the selected flow boundary, $\vec{f} = \underline{\underline{\sigma}} \cdot \vec{n}$ is the modified stress, $\underline{\underline{\sigma}} = (-p - Bo \cdot \vec{e}_g \cdot \vec{x}) \underline{\underline{I}} + Ca(\nabla \vec{u} + [\nabla \vec{u}]^T)$ is the modified stress tensor, \vec{n} is the normal pointing into the domain and c_{kj} is the tensor due to the stress jump at the boundaries ($= \delta_{kj}/2$ for smooth boundaries). G_{ij} and T_{ijk} are the two-dimensional Stokeslet and associated stress field respectively, defined as-

$$G_{ij} = -\delta_{ij} \ln |\vec{x} - \vec{x}_o| + (x_i - x_{o_i})(x_j - x_{o_j}) / (\vec{x} - \vec{x}_o)^2 \quad (5)$$

$$T_{ijk} = -4(x_i - x_{o_i})(x_j - x_{o_j})(x_k - x_{o_k}) / (\vec{x} - \vec{x}_o)^4 \quad (6)$$

This formulation allows us to use the boundary element method (BEM) [31, 32]. In the current study, we use quadratic elements to compute the integrals while solving Equation 4 (see Figure 1 for a pictorial representation of how the computational boundary is discretized into a series of quadratic elements).

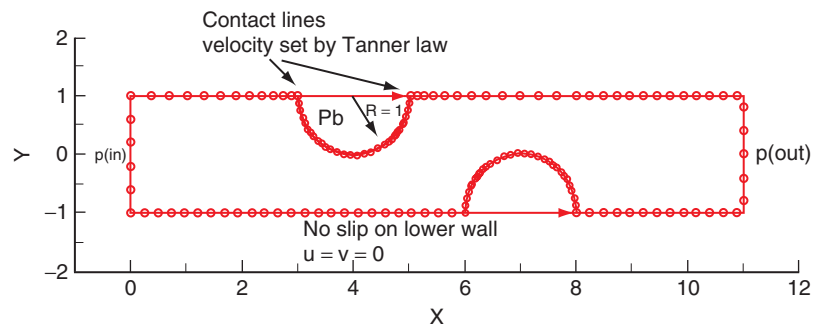


Figure 1. Computational domain for two bubbles in the channel. Every fourth grid point is shown.

5. INITIAL AND BOUNDARY CONDITIONS

Simulations have been carried out with the configuration as shown in Fig 1. The bubbles are placed symmetrically with respect to the inlet and outlet of the channel, with their centers at distances of 4 non-dimensional units and 7 non-dimensional units respectively from the left end of the channel, with the length of the channel taken as 11 non-dimensional units.

An initial pressure for the two bubbles was specified. For the current study, initial pressure in both the bubbles was set to the same value (henceforth referred to as pb). Pressure boundary conditions were specified at the inlet and outlet. Since the purpose of the present study is to investigate the effect of gravity on the evolution of bubbles, a non-dimensional pressure of 2 was imposed at both the inlet and outlet of the channel. Thus, the only forces acting on the two bubbles in our simulations were due to gravitational effects.

No-slip boundary condition was imposed at the channel walls. The motion of contact lines was modeled using the modified Tanner laws including the contact angle hysteresis [27, 28, 30]. According to modified Tanner laws, the contact line velocity u_{cl} is given as follows:

$$\begin{aligned} u_{cl} &= -k(\theta_D - \theta_A) \text{ for } \theta_D < \theta_A \\ u_{cl} &= -k(\theta_D - \theta_R) \text{ for } \theta_D > \theta_R \\ u_{cl} &= 0 \text{ for } \theta_A < \theta < \theta_R \end{aligned} \quad (7)$$

where θ_A and θ_R are the advancing and receding contact angles respectively, and θ_D is the dynamic contact angle formed between bubble surface and the channel wall. As we move away from the contact lines, the velocity on the channel wall linearly decreases to zero, i.e. no-slip boundary condition, in order to avoid singularities at the contact lines. A finite distance over which the velocity at the channel wall linearly decreases to zero is termed as the 'slip length'. According to equation (7), the contact line is stable and does not move if the dynamic contact angle (θ_D) lies between the advancing and receding contact angles. If the contact angle is not within the 'equilibrium range', the contact line moves so that the contact angle again reaches the specified range. Also, the speed of the contact line is proportional to the deviation of the dynamic contact angle from the equilibrium range. The value of the proportionality constant k in the Tanner laws equations has been taken as $k = 2.0$ and the values for the advancing and receding contact angles have been taken as $\theta_A = 50^\circ$ and $\theta_R = 70^\circ$. These values have been chosen in order to maintain the consistency of the contact angle values with previous studies [27, 28]. The stress jump at the bubble interface is given by:

$$\Delta \vec{f} = \kappa \cdot \vec{n} \quad (8)$$

where κ is the curvature of the interface and n is the normal vector at a given point on the interface. At each time step, the flow field was solved for the whole boundary and then the bubble interface was advanced in time using a simple Euler integration as described by the following kinematic boundary condition:

$$\frac{\partial \vec{Y}}{\partial t} \cdot \vec{n} = \vec{u} \cdot \vec{n} \quad (9)$$

According to this boundary condition, the interface (\vec{Y}) moves with the velocity of the fluid (\vec{u}) adjoining the interface. In this manner, after solving the flow field at each time step, the bubble interface was advanced in time and the new bubble volume was computed. The expansion and contraction of bubbles were assumed to be isothermal and the updated pressure inside the bubble was computed using the ideal gas law, according to which the product of the bubble pressure and the bubble volume is a constant. This updated pressure was then used in the stress jump condition at the interface for the next time step and thus the whole process is repeated.

6. RESULTS AND DISCUSSION

Since the blood vessels in microvasculature form a complex three-dimensional network in which different vessels have different inclinations with respect to the direction of gravity, we present here two cases of the inclination of gravity vector with respect to the channel axis to cover the two extreme possibilities: gravity acting along the channel axis and gravity perpendicular to the channel axis.

The effect of varying the strength of the gravitational forces relative to the surface tension forces has been studied by varying the Bond Number (as defined in Governing Equations section). Three values of $Bo = 0.1, 0.5$ and 1.0 - were taken in our study. A high value of Bo indicates that the system is relatively unaffected by surface tension and is dominated by the gravitational forces; a low value (typically, less than one is the requirement) indicates that surface tension dominates. We have selected these values of Bo as they bring about significant variation in bubble evolution, and are close to the actual physiological conditions.

Initial bubble pressures (pb) of 1, 2, 4 and 8 were used to carry out the simulations for different cases of Bo and gravity vector inclination. For all of the cases, simulation was run for 20 seconds, or until the bubble interface crossed the inlet or outlet boundary of the channel. Hereafter the bubble sticking to the upper wall, closer to the left end of the channel, is termed as Bubble 1 and the bubble sticking to the lower wall, closer to the right end of the channel is termed as Bubble 2. We have selected the following cases for discussion in this paper, which allow us to highlight the effects of various parameters on the bubbles' evolution and wall stresses:

- Case 1: $Bo = 0.1$, gravity perpendicular to the channel axis
- Case 2: $Bo = 1.0$, gravity perpendicular to the channel axis
- Case 3: $Bo = 0.1$, gravity along the channel axis
- Case 4: $Bo = 0.5$, gravity along the channel axis
- Case 5: $Bo = 1.0$, gravity along the channel axis

6.1. Case 1: $Bo = 0.1$, Gravity Perpendicular to the Channel Axis

The normal stresses on channel walls and the corresponding bubble interface configurations for Case 1 have been plotted at various time steps for all four cases of pb as shown in Figure 2. For gravity acting perpendicular to the channel, there is no gradient of the force field along the axis of the channel and hence, the evolution of the two bubbles is symmetric about the centre of the channel. For $pb = 1$, both the bubbles contract because of the lower pressure of the gas inside the bubble than that of the

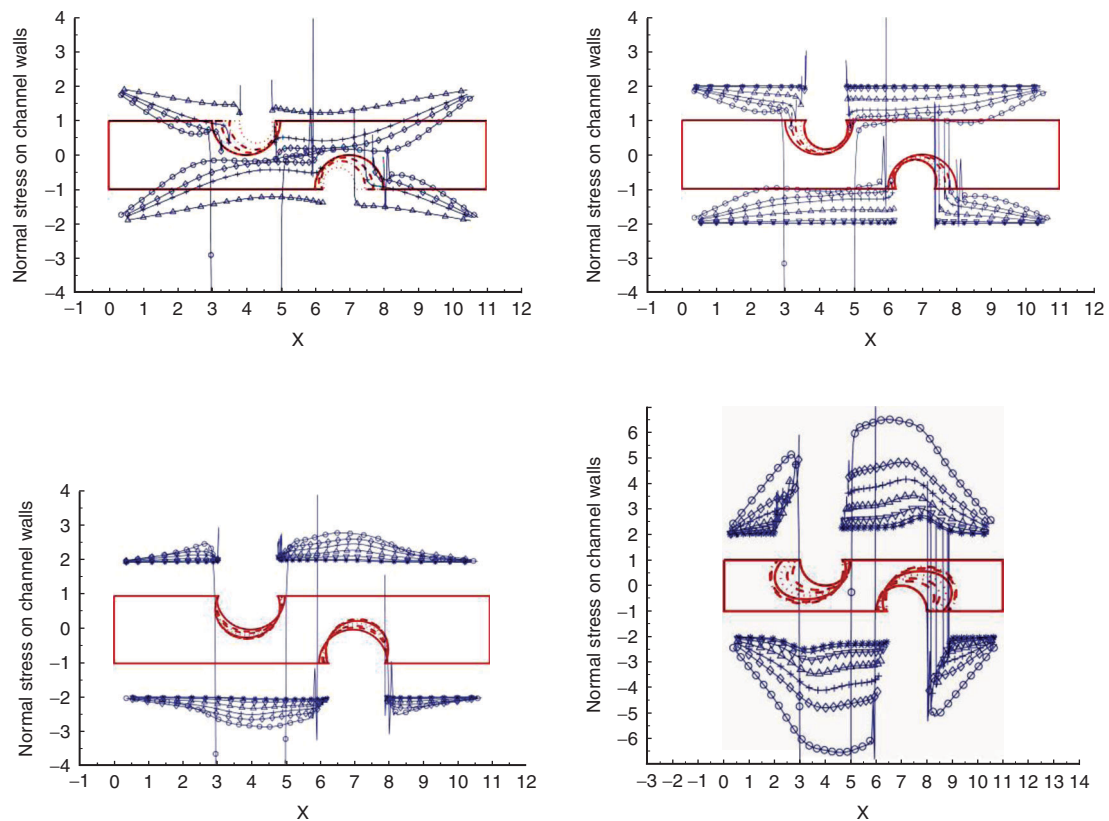


Figure 2. Evolution of bubble interface and normal stresses at $t = 0(\circ), 1(\diamond), 2(+), 4(\Delta), 8(\nabla), 14(\times)$ and $20(*)$ for $Bo = 0.1$, gravity perpendicular to the channel axis. $pb = 1$ is at top left, $pb = 2$ at top right, $pb = 4$ at bottom left and $pb = 8$ at bottom right.

surrounding fluid. Also, both the bubbles move inwards towards the centre of channel due to the inward flow of fluid from the ends of the channel as a result of the contraction of the two bubbles. For $pb = 2$, a slight contraction in both bubbles is observed. For both bubbles, the contact lines initially move inwards in order to attain the equilibrium contact angle configuration, after which they come to rest. For $pb = 4$, both the bubbles expand because the pressure inside the bubbles is higher than the pressure of the surrounding fluid. Each of the two bubbles drifts outwards while expanding due to the presence of the other expanding bubble in the vicinity. For $pb = 8$, both the bubbles rapidly expand due to a large initial bubble pressure and move towards the corresponding ends of the channel.

Had the bubbles not been in the channel, the normal stress on the wall would have uniformly been equal to 2. The presence of the bubbles results in either a positive or a negative deviation from 2 in the normal stress, depending on the bubble behavior. A contracting bubble sucks in fluid from the surroundings and thus tends to form a cusp in the normal stress profile, while an expansion results in a bulge in normal stress. When there are two bubbles inside the channel, the normal stress on the walls is the net result of the interplay between the expansion/contraction of the two bubbles. In Case 1, the evolution of the two bubbles is governed primarily by the bubble internal pressures and gravitational forces have little effect. For $pb = 1$, both the bubbles contract, resulting in low pressure in the regions surrounding the two bubbles, leading to the formation of cusps in the normal stress profile on both walls which flatten as time progresses. For $pb = 2$, the bubbles undergo a very small amount of contraction which results in almost flat normal stress curves on both the walls. The rapid expansion of the bubble for $pb = 4$ and 8 causes bulges in the normal stress profiles on the wall opposite to the bubble. Normal stresses are highest at the beginning of the simulation and decrease in magnitude with time.

Figure 3 shows the plots for shear stresses acting on the channel wall for Case 1. For $pb = 1$, both the bubbles contract towards the centre of the channel and suck the fluid in from the both ends of the channel, causing shear stresses on the channel walls. The signs of shear stress in right and left side of channel are opposite because of the opposite directions of flow. As the bubbles contract, the rate of their contraction decreases and so the flow rates and shear stresses also decrease. For $pb = 2$, the small amount of contraction in both the bubbles causes no significant flow and thus the shear stresses are very small. For $pb = 4$, the bubbles expand and we observe a reversal in the sign of shear stress on both sides of channel. For $pb = 8$, both the bubbles expand rapidly, causing large outward flow resulting in high

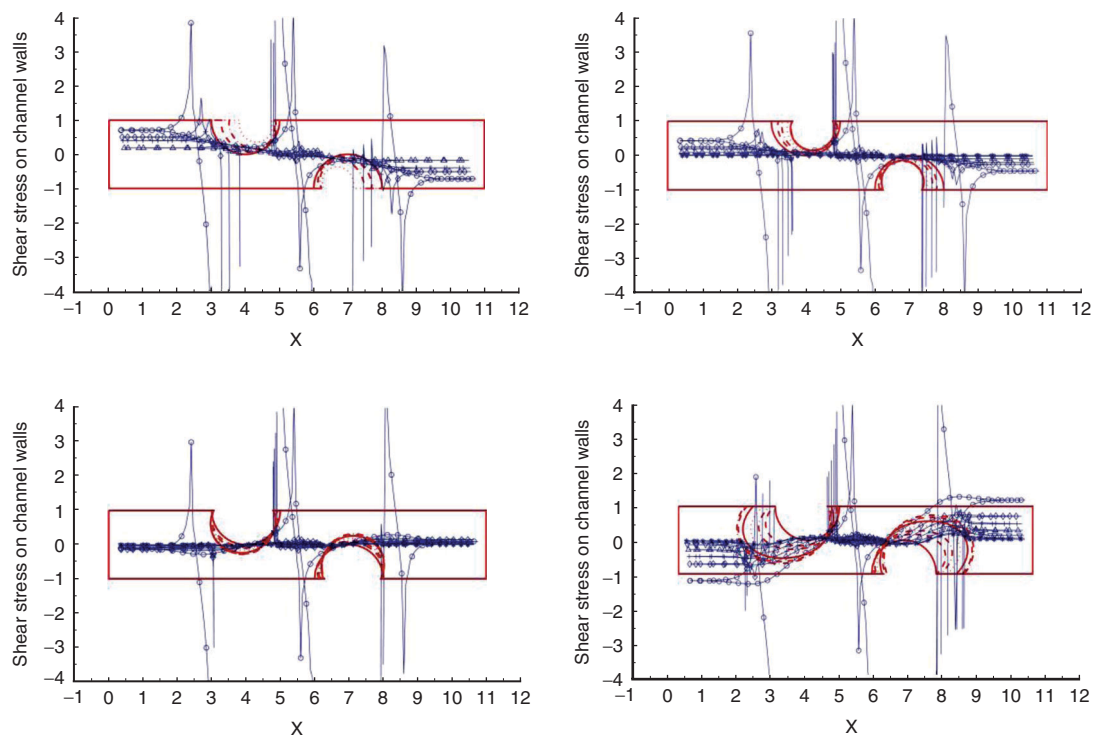


Figure 3. Evolution of bubble interface and shear stresses at $t = 0(\circ)$, $1(\diamond)$, $2(+)$, $4(\Delta)$, $8(\nabla)$, $14(\times)$ and $20(*)$ for $Bo = 0.1$, gravity perpendicular to the channel axis. $pb = 1$ is top left, $pb = 2$ is top right, $pb = 4$ is bottom left and $pb = 8$ is bottom right.

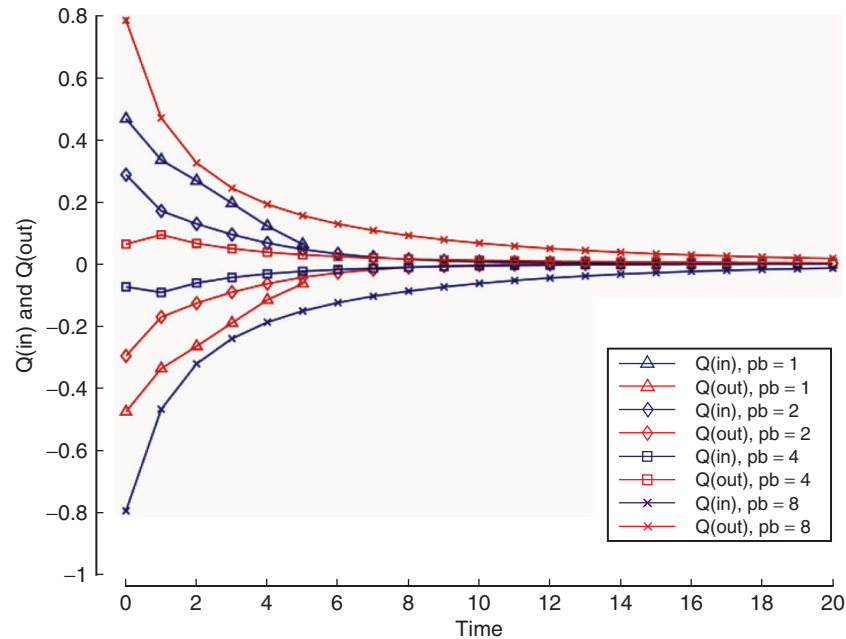


Figure 4. Flow rates vs Time for $Bo = 0.1$, gravity perpendicular to the channel axis.

shear stresses in the channel. It should be noticed that the shear stress in the region between the two bubbles remains close to zero because of negligible flow in this region. Similar to the trend in normal stresses, the magnitude of shear stresses is highest at the beginning and decreases with time.

Flow rates through the left and right ends of the channel for Case 1 are shown in Figure 4. The flow rate through the left part of the channel is denoted by $Q(\text{in})$ and that through the right end is denoted by $Q(\text{out})$. By convention, the flow from left to right along the channel axis is positive. For $pb = 1$, the bubbles contract and suck in fluid from both ends of the channel. Hence there is positive flow at the left end of the channel and negative flow at the right end. The magnitude of both $Q(\text{in})$ and $Q(\text{out})$ decreases with time as the bubbles slowly achieve equilibrium with the surrounding fluid. For $pb = 2$, the contraction in the bubbles is reduced and hence the flow rates also decrease in magnitude. For $pb = 4$, bubbles expand and push fluid out of the channel, due to which the flow direction changes from inwards to outwards. The magnitude of flow rates for $pb = 4$ is small because there is only a small amount of expansion. For $pb = 8$, high initial flow rates are observed which decrease with time as the bubbles achieve equilibrium with the surroundings.

6.2. Case 2: $Bo = 1.0$, Gravity Perpendicular to the Channel Axis

A high value of Bond number results in a much stronger effect of gravity on the bubble evolution in Case 2 than that in Case 1. Figure 5 shows the bubble evolution and normal stresses for Case 2. In all four cases of pb , the contact lines of Bubble 2 come closer to each other than those of Bubble 1. Bubble 2 expands upwards for $pb = 4$ and 8.

The effect of gravitational forces is most visible for $pb = 4$ and 8. For $pb = 4$, two opposing effects act on Bubble 1. The internal bubble pressure tries to force the bubble to expand while the buoyant forces act against that expansion. The result is a very small expansion of Bubble 1, leaving its contact lines almost stationary. On the other hand both buoyancy and initial bubble pressure act together on Bubble 2, causing it to expand upwards rapidly. The bubble takes an elongated shape as shown in Figure 5. For $pb = 8$, both the bubbles expand rapidly because of the high initial pressure. While Bubble 1 undergoes more spread because of the buoyant forces pressing on the interface from below, Bubble 2 gets stretched upwards and expands until it comes within the vicinity of the upper wall, after which it gets flattened.

While most aspects of the nature of the normal stress profile for Case 2 are similar to those for Case 1, there are some significant differences which arise due to the high value of Bo . In all cases of pb , there is a localized bulge in the normal stress profile opposite to Bubble 2 on the upper wall. This bulge is most prominent for $pb = 8$, present even at high values of time, showing that Bubble 2 keeps expanding rapidly even after Bubble 1 has stopped expanding. This illustrates the effect of gravity acting perpendicular to the channel, which, while dampening the expansion of Bubble 1, causes a sustained expansion in Bubble 2.

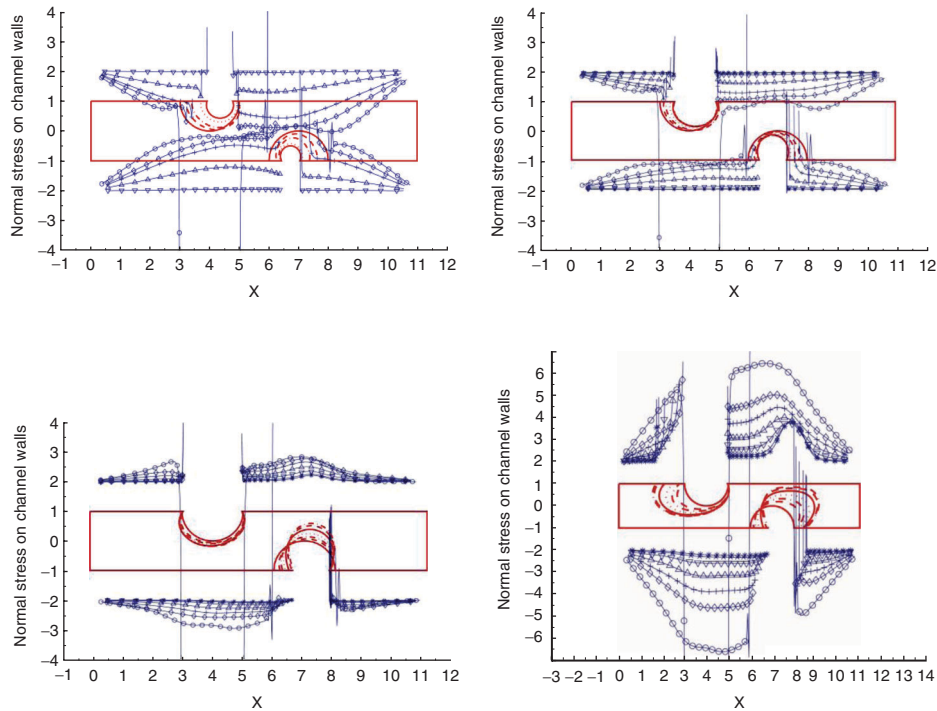


Figure 5. Evolution of bubble interface and normal stresses at $t = 0(\circ)$, $1(\diamond)$, $2(+)$, $4(\Delta)$, $8(\nabla)$, $14(\times)$ and $20(*)$ for $Bo = 1.0$, gravity perpendicular to channel axis. $pb = 1$ is top left, $pb = 2$ is top right, $pb = 4$ is bottom left and $pb = 8$ is bottom right.

The shear stresses for Case 2 are shown in Figure 6. Except for a slight difference in the magnitudes of shear stresses in the right and left parts of the channel, no significant effect of the high Bond number is observed and the plots are similar to the corresponding plots for Case 1. This indicates that even though the presence of gravity alters the evolution of the bubbles, suppressing the expansion of Bubble 1 and aiding the expansion of Bubble 2, the nature of the flows inside the channel is not affected significantly. Thus the both the magnitudes and temporal evolution of shear stresses stay similar to Case 1.

Similar to shear stresses, the flow rate profiles for Case 2 look similar to those for Case 1. There is inward flow from both ends of the channel for $pb = 1, 2$ and outward flow for $pb = 4$ and 8 . Possibly due to elongation of Bubble 2 for $pb = 4$ and suppressed expansion of Bubble 1, outward flow from the left end is somewhat reduced in the beginning.

6.3. Case 3: $Bo = 0.1$, Gravity Along the Channel Axis

The smallness of Bo for this case dictates that the evolution of bubbles is still dominated by the initial bubble pressure and gravity has a minor role to play. Figure 8 shows the normal stress plots on channel walls and the corresponding bubble interface configurations at various time steps for Case 3. The behavior of the bubbles is similar to Case 1. For $pb = 1$, both the bubbles contract and move inwards towards the centre of channel. For $pb = 2$, both bubbles contract little because the initial bubble pressure is close to surrounding fluid pressure. A slight asymmetry is observed in the movement of the bubbles as the inward movement of Bubble 2 is less than Bubble 1. This asymmetry owes its origin to the presence of the gravitational field in the system, which, though small, causes buoyant forces acting from left to right to be exerted on the bubbles. For $pb = 4$, both the bubbles expand and drift outwards due to the presence of the other expanding bubble in the vicinity. The asymmetry in evolution is more evident in this case as compared to the cases with $pb = 1$ and 2 . Bubble 2 expands more than Bubble 1. In the case with $pb = 8$, the bubbles expand rapidly towards the ends of channel. Similar to the case with $pb = 4$, Bubble 2 expands to a greater volume than Bubble 1. Both the bubbles are flattened as they approach the opposite wall. In the case of Bubble 2, at every time step, the right contact line makes a contact angle with the wall which is smaller than the advancing contact angle, causing the contact line to move towards the right. As the contact line moves, the interface moves to the right due to expansion. The contact line is unable to reach an

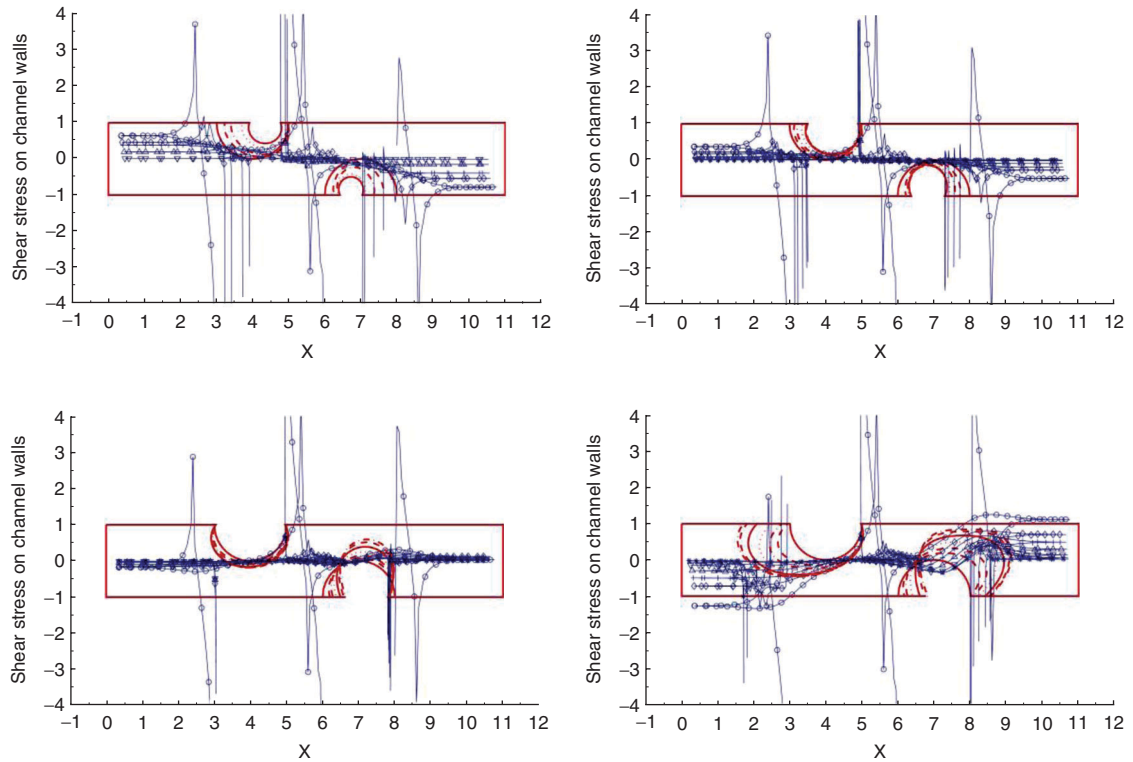


Figure 6. Evolution of bubble interface and shear stresses at $t = 0(\circ)$, $1(\diamond)$, $2(+)$, $4(\Delta)$, $8(\nabla)$, $14(\times)$ and $20(*)$ for $Bo = 1.0$, gravity perpendicular to the channel axis. $pb = 1$ is at top left, $pb = 2$ at top right, $pb = 4$ at bottom left and $pb = 8$ at bottom right.

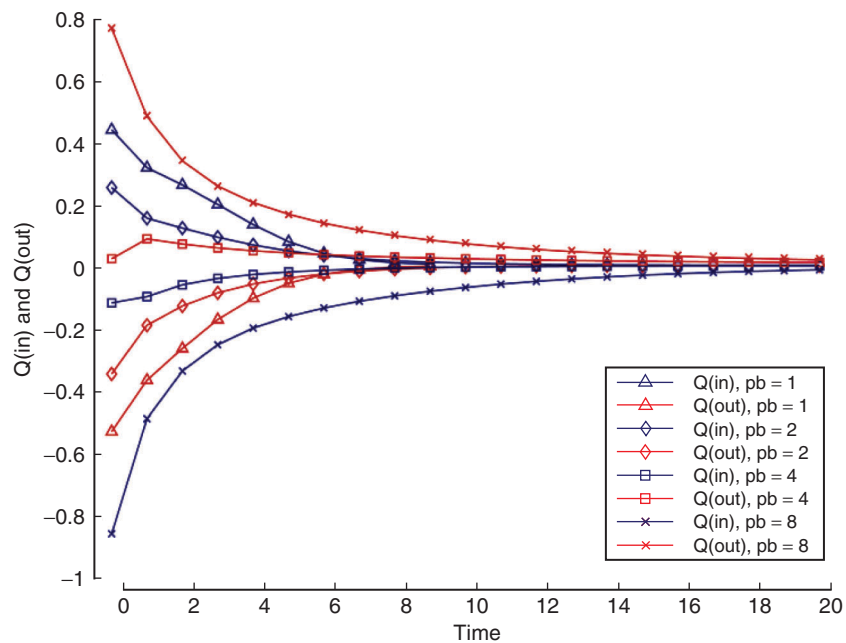


Figure 7. Flow rate vs Time for $Bo = 1.0$, gravity perpendicular to the channel axis.

equilibrium contact angle and hence keeps moving. For Bubble 1, the right contact line moves a little to the left and attains the equilibrium position, so the bubble becomes lodged at that position and the contact line does not move any further.

The plots of normal stress for Case 3 are also similar to those for Case 1. For $pb = 1$ and 2 , both the bubbles contract, causing cusps in the normal stress profile on both walls. For $pb = 4$ and 8 , the

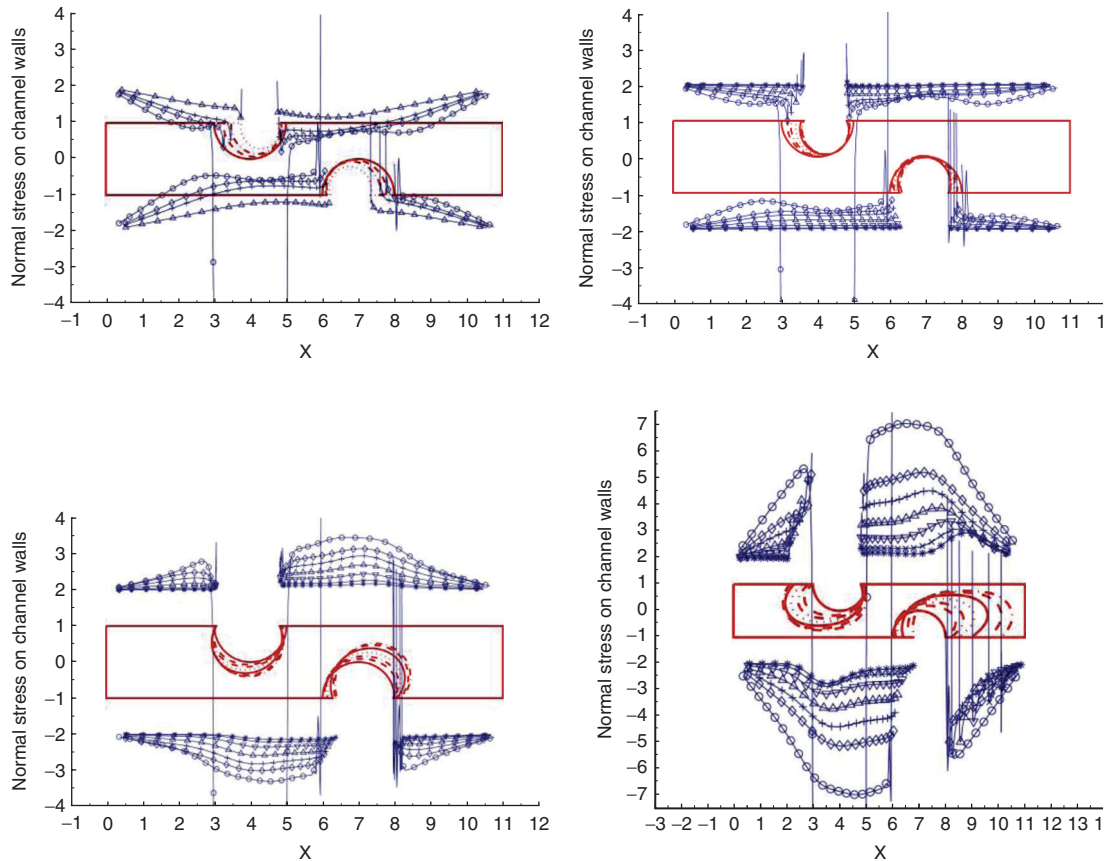


Figure 8. Evolution of bubble interface and normal stresses at $t = 0(\circ)$, $1(\diamond)$, $2(+)$, $4(\Delta)$, $8(\nabla)$, $14(\times)$ and $20(*)$ for $Bo = 0.1$ and gravity along the channel axis. $pb = 1$ is top left, $pb = 2$ is top right, $pb = 4$ is bottom left and $pb = 8$ is bottom right.

expansion in the bubbles causes bulges in the normal stress profiles on the walls. The magnitudes of the normal stresses caused by contraction or expansion of the bubbles are greatest at the beginning of the simulation and decrease as time progresses.

Figure 9 shows the plots for shear stresses acting on the channel wall for Case 3. The shear stress profiles for Case 3 are also similar to those for Case 1. For $pb = 1$ and 2, positive shear acts on the left part of the channel and negative on the right part of the channel, the strength of which reduces as time elapses. The shear stresses change sign when bubbles behavior changes from contraction to expansion with $pb = 4$. High initial shear stresses are observed on the channel walls for $pb = 8$ which reduce as time progresses because of the reduced rate of expansion.

Qualitatively, the flow rate profiles for Case 3, as shown in Figure 10, are also similar to those for Case 1. For $pb = 1, 2$ when bubbles contract, there is inward flow at both ends of the channel and for $pb = 4$ and 8 there is outward flow because of expanding bubbles. The initial inward flow rates for $pb = 1, 2$ are smaller than for the case with $Bo = 0.1$ and gravity perpendicular to the channel axis while the outward flow rates for $pb = 4$ and 8 are larger. For $pb = 8$, there is a net outflow even at the end of simulation indicating that Bubble 2 is still expanding.

6.4. Case 4: $Bo = 0.5$, Gravity Along the Channel Axis

The effect of increased strength of gravity acting along the channel axis on the bubble evolution and normal stress plots in this case can be seen in Figure 11, which shows the normal stress profiles and bubble interface configuration at various time steps for Case 4. For $pb = 1$, Bubble 1 exhibits a small amount of contraction while Bubble 2 undergoes expansion and moves towards the right. In the case of $Bo = 0.5$, a sufficiently strong gravitational field acts on the system, setting up a hydrostatic pressure gradient along the length of the channel which decreases along the length of the channel, reaching a minimum at the right end. Bubble 1 contracts because of higher hydrostatic pressure in the left part of

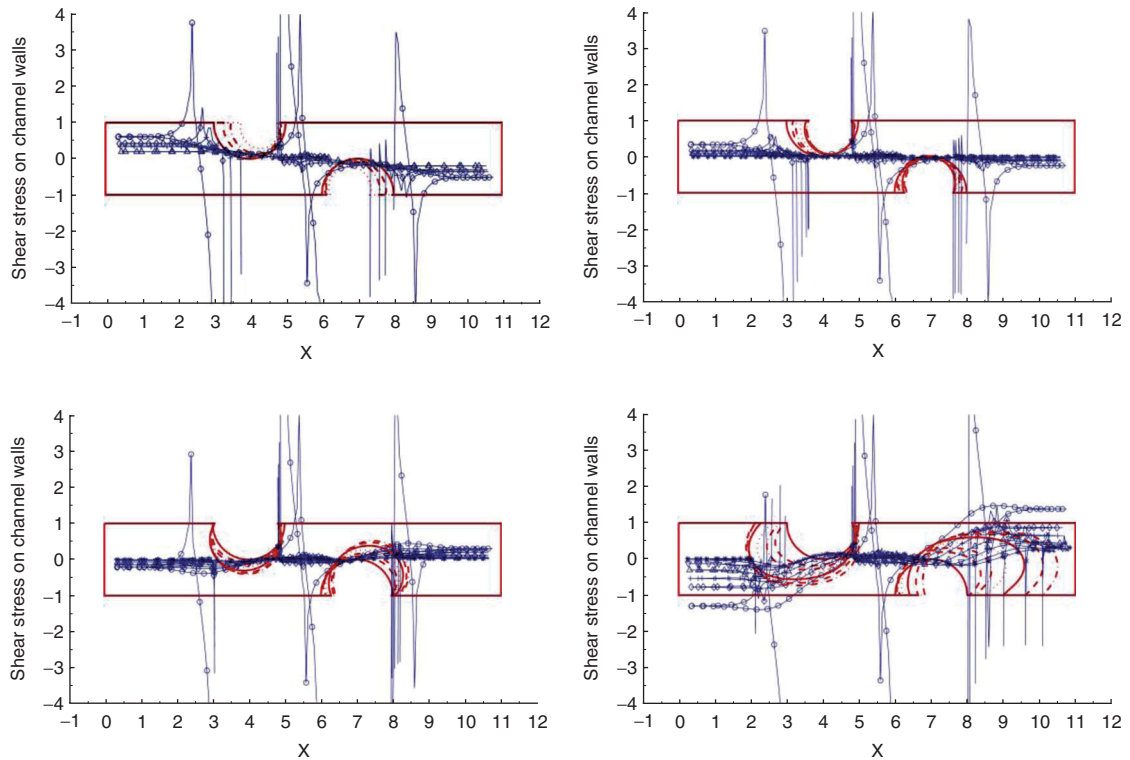


Figure 9. Evolution of bubble interface and shear stresses at $t = 0(\circ)$, $1(\diamond)$, $2(+)$, $4(\Delta)$, $8(\nabla)$, $14(\times)$ and $20(*)$ for $Bo = 0.1$, gravity along the channel axis. $pb = 1$ is top left, $pb = 2$ is top right, $pb = 4$ is bottom left and $pb = 8$ is bottom right.

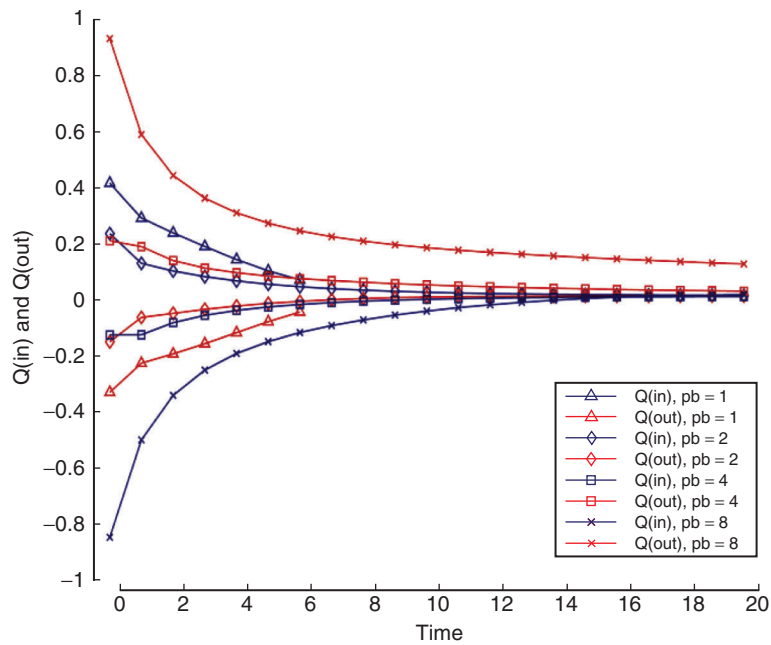


Figure 10. Flow rate vs Time for $Bo = 0.1$, gravity along the channel axis.

channel. On the other hand, Bubble 2 is in a region of lower hydrostatic pressure, causing it to expand and move to the right because of its buoyancy. The configurations for which the bubble interface is in very close proximity to the end of channel have not been considered for this study.

For $pb = 2$, Bubble 1 does not contract or expand, while Bubble 2 expands at a rate much higher than in the case with $pb = 1$. For $pb = 4$, both bubbles expand, with the rate of expansion of Bubble 2 being

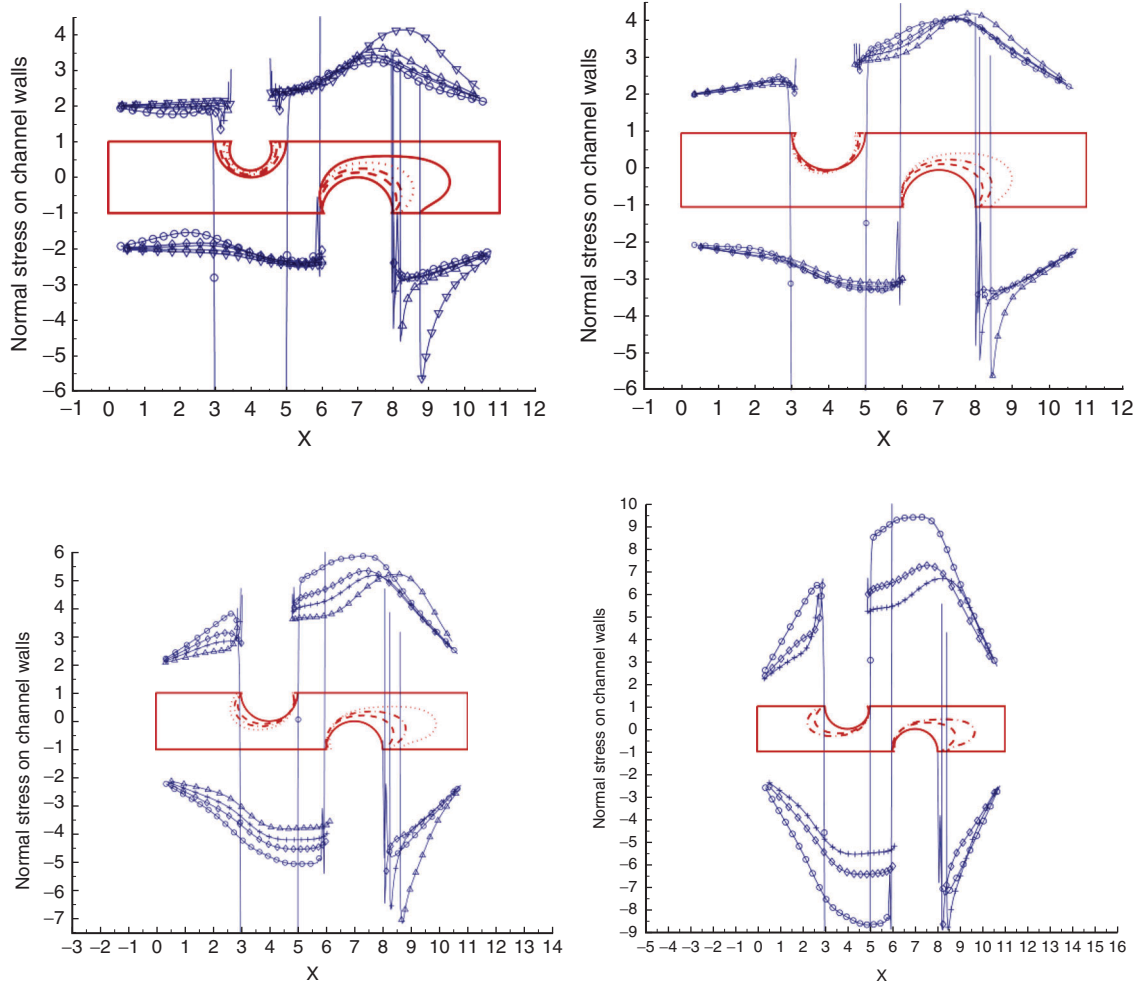


Figure 11. Evolution of bubble interface and normal stresses at $t = 0(\circ)$, $1(\diamond)$, $2(+)$, $4(\Delta)$ and $8(\nabla)$ for $Bo = 0.5$, gravity along channel axis. $pb = 1$ is top left, $pb = 2$ is top right, $pb = 4$ is bottom left and $pb = 8$ is bottom right.

much higher than in the previous cases. For $pb = 8$, both the bubbles expand rapidly and drift towards opposite ends of the channel. In all four cases of pb , elongation of Bubble 2 is observed along the channel axis. On comparing the bubble evolution in Case 4 with Case 3, we find that while for Case 3, the evolution of the bubbles was primarily governed by the initial bubble pressures alone, for Case 4, the increased strength of gravity results in a hydrostatic pressure field in the channel, and thus the role of gravity becomes of greater significance.

For Case 4, Bubble 2 undergoes a large amount of expansion in all the different cases of initial bubble pressure, due to which we observe high normal stress in the right part of the channel as compared to the left part as seen in Fig 8. For $pb = 1$, while Bubble 1 contracts, resulting in cusps in the normal stress profile, Bubble 2 expands and results in high normal stresses in the right part of the channel. For $pb = 2, 4$ and 8 , Bubble 1 also expands, thus causing an outward bulge in the normal stress profile. As pb increases, the rate of expansion of the bubbles and hence the initial and overall magnitude of normal stresses on the walls also increases.

Shear stress plots for Case 4 are shown in Figure 12. For $pb = 1$, Bubble 1 contracts while Bubble 2 expands towards its right. As a result, fluid is drawn into the channel from the left by Bubble 1 while it is pushed out though the right by Bubble 2. Positive initial shear stress is observed on both sides of the channel, the magnitude of the stress being higher on the right side. The shear stress in the region between the two bubbles remains close to zero. For $pb = 2$, Bubble 1 remains almost unchanged in size while Bubble 2 expands, causing outward flow and therefore high shear stress in that region. For $pb = 4$ and 8 , both the bubbles expand and cause outward flows. Thus oppositely signed shear stress profiles are observed on the two sides of the channel.

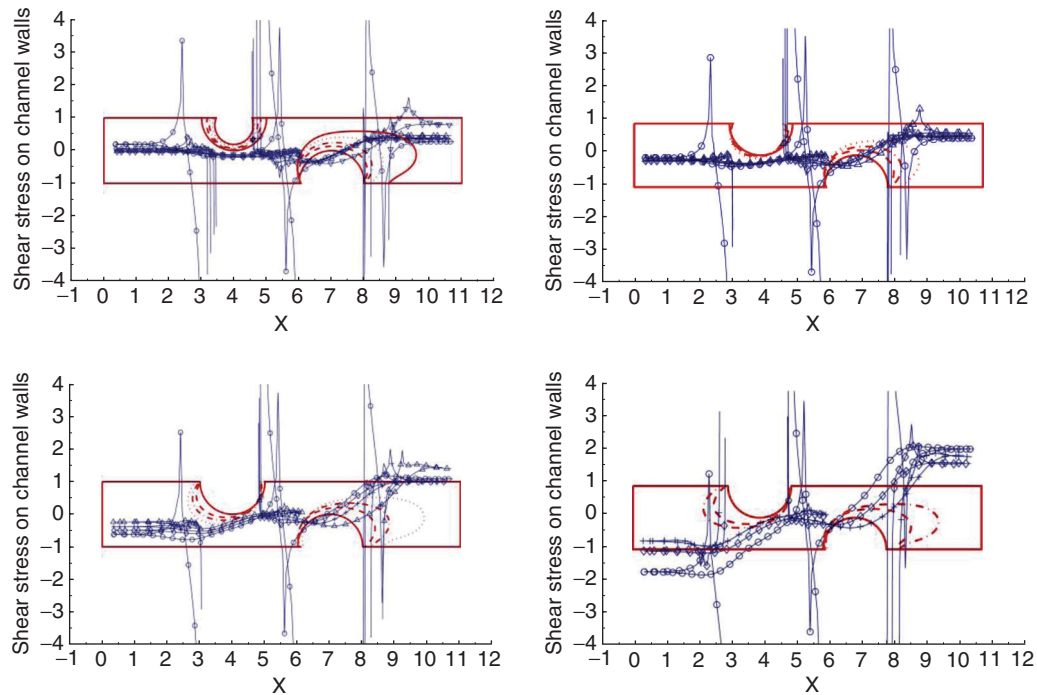


Figure 12. Evolution of bubble interface and shear stresses at $t = 0(\circ)$, $1(\diamond)$, $2(+)$, $4(\Delta)$ and $8(\nabla)$ for $Bo = 0.5$, gravity along the channel axis. $pb = 1$ is top left, $pb = 2$ is top right, $pb = 4$ is bottom left and $pb = 8$ is bottom right.

Figure 13 shows the flow rates for Case 4. Bubble 2 expands for all cases of pb and causes outward flow from both ends of the channel. For $pb = 1$, as Bubble 1 contracts and Bubble 2 expands, there is a small inward flow from the left end in the beginning which dies out very quickly. There is outward flow from the right end of the channel which slowly increases, indicating that the rate of expansion of Bubble 2 increases. For the cases of $pb = 2, 4$ and 8 , there is initial outward flow at the left end of the channel which decreases with time while the outward flow from the right end increases with time as Bubble 2 expands. The magnitude of the outward flow increases with increase in pb .

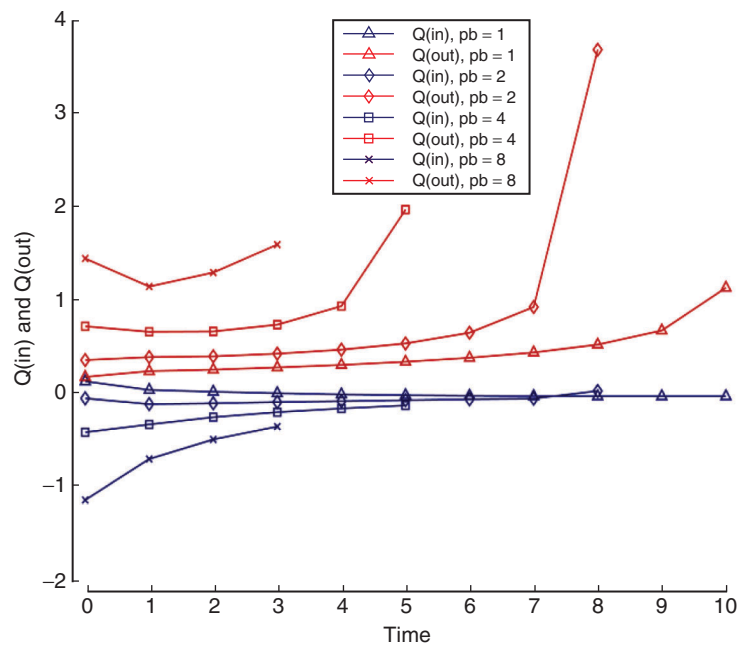


Figure 13. Flow rate vs Time for $Bo = 0.5$, gravity along the channel axis.

6.5. Case 5: $Bo = 1.0$, Gravity Along the Channel Axis

For Case 5, a pronounced effect of gravity is observed on the bubble behavior and wall stresses, evident from the bubble evolution and normal stress plots shown in Figure 14. For $pb = 1$, Bubble 1 contracts slightly while Bubble 2 expands at a rapid rate, stretching towards the right end of the channel. As Bubble 2 expands, it pushes the fluid around it and Bubble 1 drifts to the left. For $pb = 2$, Bubble 1 expands and moves to the left. The rate of expansion of Bubble 2 is higher than the case with $pb = 1$. For $pb = 4$, both the bubbles expand rapidly and Bubble 1 drifts more rapidly towards its left. Similar behavior with a much higher rate of expansion of the bubbles is observed for $pb = 8$. On comparison with the corresponding cases with $Bo = 0.1$ and 0.5 , it can be seen that the present case with $Bo = 1.0$ has the most dominant effect of the gravitational forces. The rates of expansion of the bubbles are highest in this case. A strong hydrostatic pressure field, formed due to gravity, governs the behavior of the bubbles and causes their expansion.

A high rate of expansion of the two bubbles results in very high normal stresses on the channel walls. In all four cases of initial bubble pressure, Bubble 2 undergoes rapid expansion, as a result of which, there is very high normal stress in the right part of channel. As pb increases, the rate of expansion of the bubbles, and consequently the magnitude of normal stress on the channel walls, increase.

Similar to the normal stresses, very high shear stresses acting on the channel wall are observed in Case 5, as can be seen in Figure 15. High flow rates set up inside the channel by the rapid expansion

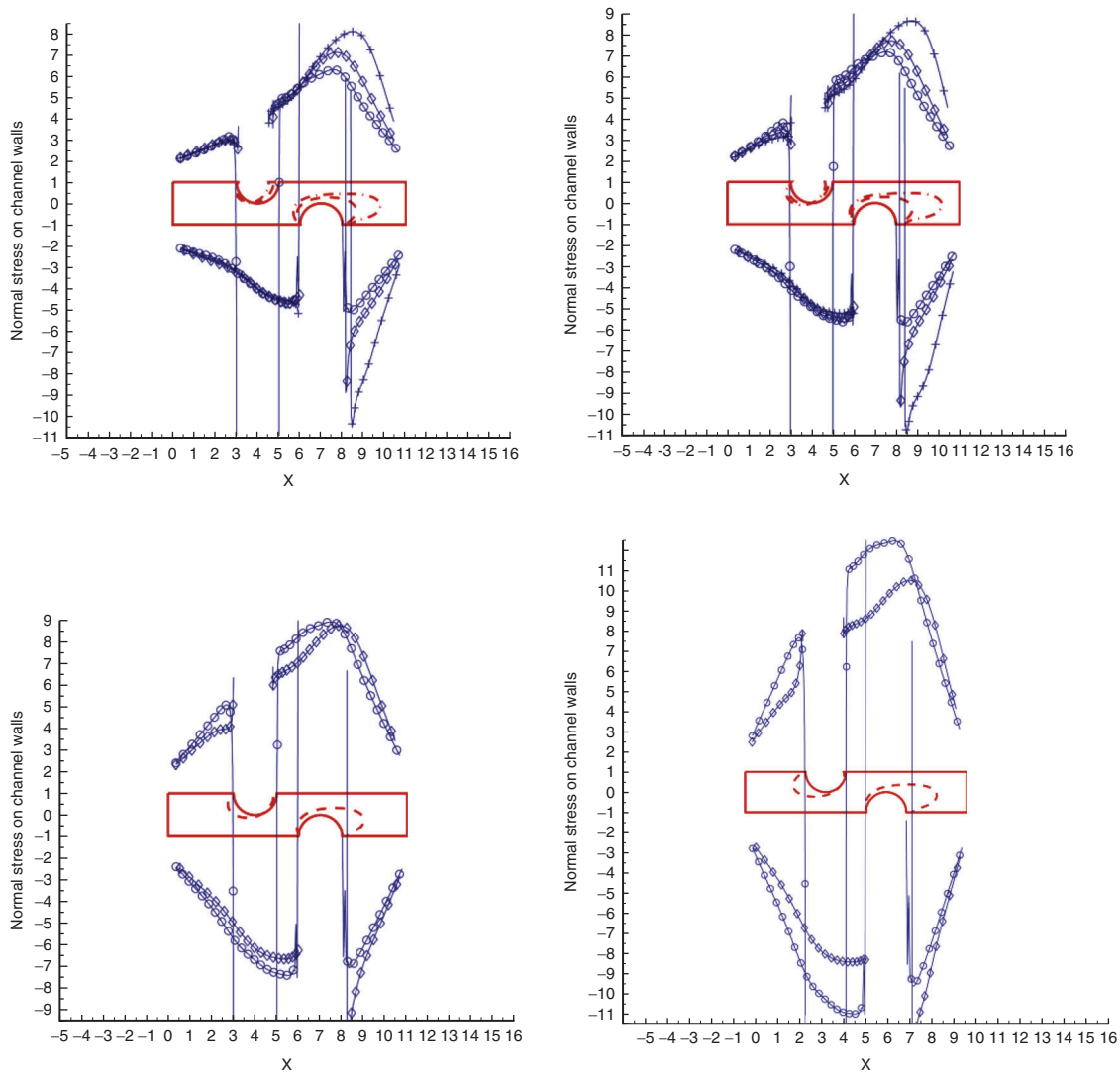


Figure 14. Evolution of bubble interface and normal stresses at $t = 0(\circ)$, $1(\diamond)$ and $2(+)$ for $Bo = 1.0$, gravity along channel axis. $pb = 1$ is top left, $pb = 2$ is top right, $pb = 4$ is bottom left and $pb = 8$ is bottom right.

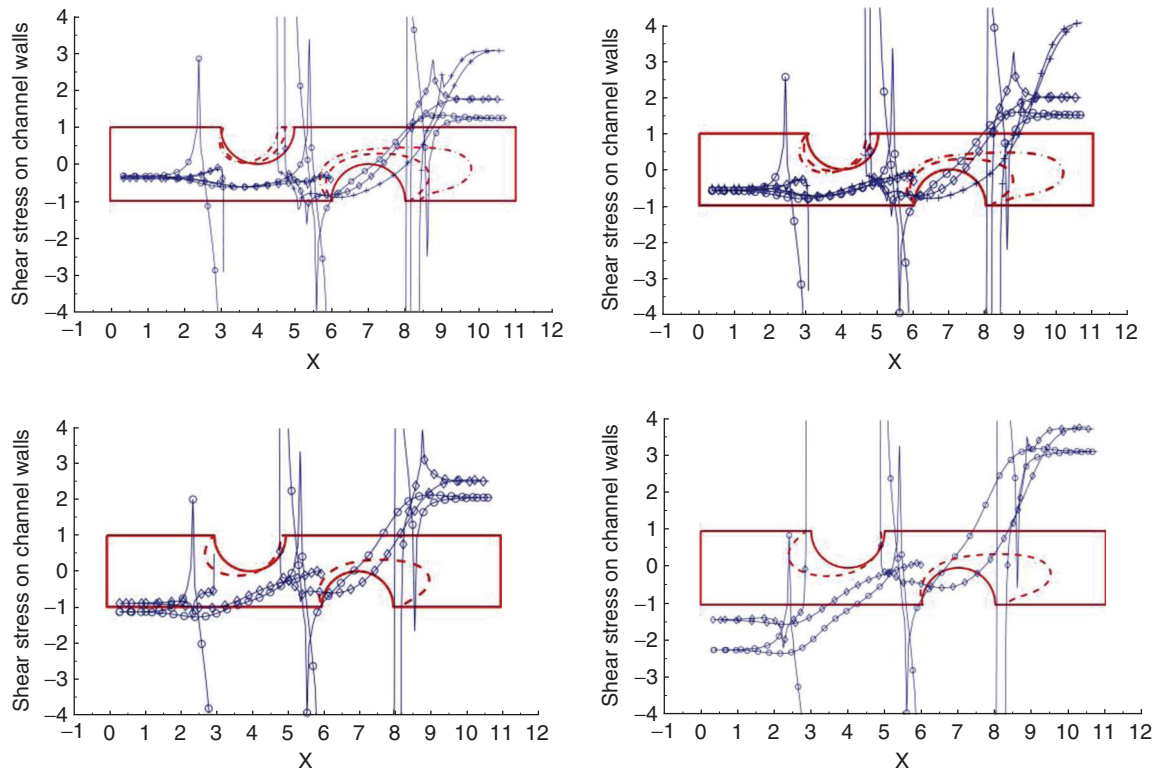


Figure 15. Evolution of bubble interface and shear stresses at $t = 0(\circ)$, $1(\diamond)$ and $2(+)$ for $Bo = 1.0$, gravity along the channel axis. $pb = 1$ is top left, $pb = 2$ is top right, $pb = 4$ is bottom left and $pb = 8$ is bottom right.

of the bubbles result in high shear on the walls. In all the four cases of initial bubble pressure, shear stresses in the right part of the channel are higher than those on the left.

Figure 16 shows flow rates for Case 5. The flow rate profiles for Case 5 are similar to those observed in Case 4, except that the magnitudes of flow rate are much higher in this case. In all cases, there is

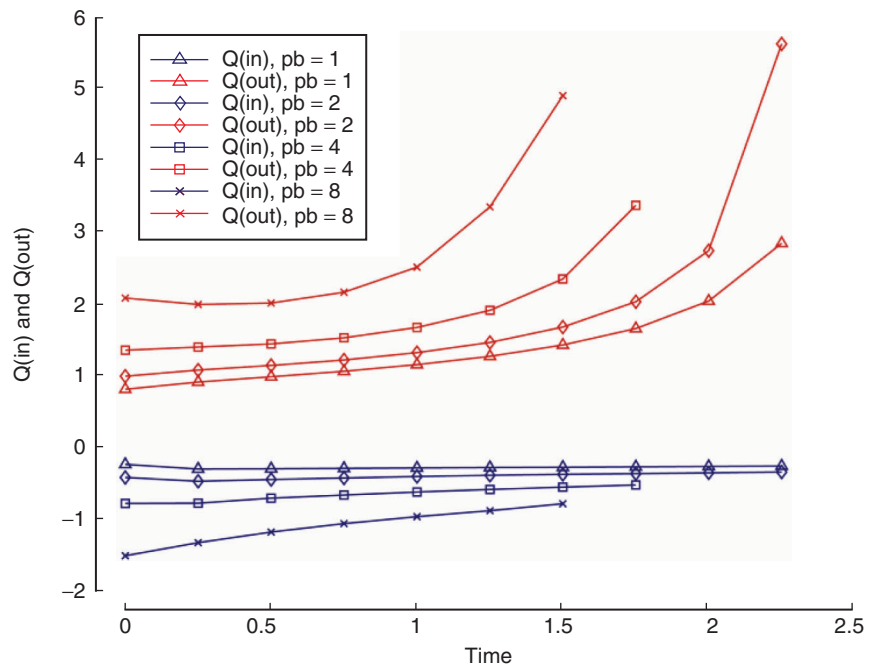


Figure 16. Flow rate vs Time for $Bo = 1.0$, gravity along the channel axis.

outward flow from both ends of the channel with outward flow from the left end decreasing with time and flow from the right end swiftly increasing as Bubble 2 expands.

7. CONCLUSIONS AND FUTURE WORK

The work presented in this paper is the first attempt made to computationally study the behavior of multiple bubbles sticking and sliding along microvessel walls. The role of both the strength and the inclination of the microvessel with respect to gravity were examined. Flow inside the channel was modeled using Stokes Equation for an incompressible flow including the terms resulting from gravitational forces and was solved using an iterative algorithm with moving interfaces. Motion of the three-phase contact line was modeled using Tanner laws including contact angle hysteresis. Our simulations show a strong effect of gravity on the evolution of the bubbles and thus indicate that the role of gravity should be considered in future studies concerning embolotherapy.

It was found that the tendency of the bubbles to become lodged at a particular location inside the channel was highest when the channel was placed perpendicular to gravity, i.e. horizontally. The other extreme, i.e., when the channel was aligned with the direction of gravity, was investigated and it was found that even at low strength of gravity (low value of Bo), there was some sliding of the bubbles on the channel walls, which could prevent them from lodging in the channel. The sliding behavior of the bubbles increased with the increase in Bo due to the action of buoyant forces. At high values of Bo , swift expansion of the bubble on the right was observed which resulted in high magnitudes of normal and shear stress on the channel walls. This is expected because with increase in the strength of gravity, the magnitude of buoyant forces increases, as does the gradient in hydrostatic pressure. This causes the gas bubbles to move towards regions of lower pressure even more rapidly. Consistent with the results of Eshpuniyani *et al.* [28], the peaks of shear stress were found on the contact lines which could potentially result in damage to the endothelial membrane and thus are a matter of major concern. Since the two bubbles were closely spaced, they interacted strongly with each other and affected each other's evolution. The sudden expansion of one bubble caused contraction and sliding of the other bubble as was seen in the cases with $Bo = 0.5$ and 1.0 .

In all cases, we found that the magnitudes of the wall normal and shear stresses were highest at the beginning of the simulation and decreased with time, consistent with the findings of Eshpuniyani *et al.* [28] and Ye and Bull [2]. We also examined the variation of flow rates with time at both ends of the channel and found that it was strongly correlated with the expansion/contraction of the two bubbles.

The current work investigates the role of gravity in the evolution of multiple bubbles inside the microvasculature without considering the effect of background pressure. In reality, there is a pressure-driven background flow which may or may not be pulsatile. It remains to be investigated how the bubbles behave in presence of both a background flow and gravity. Apart from pressure-driven background flow, several assumptions will have to be relaxed in order to make the model more realistic. Factors that would have to be incorporated in future studies include the non-Newtonian nature of blood, wall surface properties, wall flexibility and the particulate nature of blood.

The present study is applicable only to cases in which the bubble is already sticking/attached to the channel wall. It would be useful to model the process of a bubble coming in contact with the wall and then sticking to it. Such a model could then be combined with a simulation of bubble formation (similar to the simulations carried out by Ye and Bull [2]) and a model for bubbles sticking to the channel walls in the presence of both pressure and gravity, enabling the entire process of bubble formation and lodging to be simulated from beginning to end.

ACKNOWLEDGEMENTS

This work was supported by NIH grants R01EB006476. The authors wish to thank Nandini Ramesh for critical reading of the manuscript.

REFERENCES

- [1] Bull, J.L., Cardiovascular Bubble Dynamics, Critical Reviews in Biomedical Engineering, 2005, 33(4) 299–346.
- [2] Ye, T., Bull, J. L., Direct Numerical Simulations of Micro-bubble Expansion in Gas Embolotherapy, Journal of Biomechanical Engineering, 2004, 126(6) 745–759.

- [3] Kripfgans, O.D., Fowlkes, J.B., Miller, D.L., Eldevik, O.P., and Carson, P.L., Acoustic Droplet Vaporization for Therapeutic and Diagnostic Applications, 2000, *Ultrasound in Medicine & Biology*, 2000, 26(7), 1177–1189.
- [4] Kripfgans, O.D., Fowlkes, J.B., Woydt, M., Eldevik, O.P., Carson, P.L., In Vivo Droplet Vaporization for Occlusion Therapy and Phase Aberration Correction, *IEEE Transactions on Ultrasonics Ferroelectrics And Frequency Control*, 2002, 49(6), 726–738.
- [5] Kripfgans, O.D., Fabiili, M.L., Carson, P.L., Fowlkes, J.B., On the Acoustic Vaporization of Micrometer-sized Droplets, *Journal of the Acoustical Society of America*, 2004, 116(1), 272–281.
- [6] Cavanagh, D.P., Eckmann, D.M., Interfacial Dynamics of a Stationary Gas Bubble in Flows in Inclined Tubes, *Journal of Fluid Mechanics*, 1999, 398, 225–244.
- [7] Cavanagh, D.P., Eckmann, D.M., The Effects of Soluble Surfactant on the Interfacial Dynamics of a Stationary Bubble in Inclined Tubes, *Journal of Fluid Mechanics*, 2002, 469, 369–400.
- [8] Maneri, C.C., Zuber, N., An Experimental Study of Plane Bubbles Rising at an Inclination, *International Journal of Multiphase Flow*, 1974, 1, 623–645.
- [9] Masliya, J., Jauhari, R., Gray, M., Drag Coefficients for Air Bubbles rising along an Inclined Surface, *Chemical Engineering Science*, 1994, 49(12), 1905–1911.
- [10] Maxworthy T., Bubble Rise under an Inclined Plate, *Journal of Fluid Mechanics*, 1991, 229, 659–674.
- [11] Tsao, H.K., Koch, D.L., Observations of High Reynolds Number Bubbles Interacting with a Rigid Wall, *Physics of Fluids*, 1997, 9 (1), 44–56.
- [12] Zukoski, E.E., Influence of Viscosity, Surface Tension and Inclination Angle on Motion of Long Bubbles in Closed Tubes, *Journal of Fluid Mechanics*, 1966, 25(4), 821–837.
- [13] Eshpuniyani, B., Fowlkes, J.B., Bull, J.L., A Bench Top Experimental Model of Bubble Transport in Multiple Arteriole Bifurcations, *International Journal of Heat and Fluid Flow*, 2005, 26(6), 865–872.
- [14] Lelkes, P. I., *Mechanical Forces and the Endothelium*, Harwood, Amsterdam, 1999.
- [15] Dewey, Jr., C.F., Bussolari, S.R., Gimbrone, Jr., M.A., Davies, P.F., The Dynamic Response of Vascular Endothelial Cells to Fluid Shear Stress, *ASME Journal of Biomechanical Engineering*, 1981, 103(3), 177–185.
- [16] Nerem, R.M., Levesque, M.J., and Cornhill, J.F., Vascular Endothelial Morphology as an Indicator of the Pattern of Blood Flow, *ASME Journal of Biomechanical Engineering*, 1981, 103(3), 172–176.
- [17] Levesque, M.J., and Nerem, R.M., The Elongation and Orientation of Cultured Endothelial Cells in Response to Shear Stress, *ASME Journal of Biomechanical Engineering*, 1985, 107(4), 341–347.
- [18] Franke, R.P., Grafe, M., Schnittler, H., Seiffge, D., Mittermayer, C., and Drenckhahn, D., Induction of Human Vascular Endothelial Stress Fibers by Fluid Shear Stress, *Nature*, 1984, 307, 648–649.
- [19] Kim, D.W., Gotlieb, A.I., and Langille, B.L., In Vivo Modulation of Endothelial f-Actin Microfilaments by Experimental Alterations in Shear Stress, 1989, *Atherosclerosis*, 9, 439–445.
- [20] Ookawa, K., Sato, M., and Ohshima, N., Changes in the Microstructure of Cultured Porcine Aortic Endothelial Cell in the Early Stage After Applying a Fluid-Imposed Shear Stress, *ASME Journal of Biomechanical Engineering*, 1992, 25(11), 1321–1328.
- [21] Olesen, S. P., Clapham, D. E., and Davies, P. F., Haemodynamic Shear Stress Activates a K⁺ Current in Vascular Endothelial Cells, *Nature*, 1988, 331, 168–170.
- [22] Davies, P.F., Robotewskyj, A., Griem, M.L., Dull, R.O., and Polacek, D.C., Hemodynamics Forces and Vascular Cell Communication in Arteries, *Archives of Pathology & Laboratory Medicine*, 1992, 116(12), 1301–1306.
- [23] Davies, P.F., and Tripathi, S.C., Mechanical Stress Mechanisms and the Cell: an Endothelial Paradigm, *Circulation Research*, 1993, 72, 239–245.
- [24] Nollert, M.N., Diamond, S.L., and McIntire, L.V., Hydrodynamic Shear Stress and Mass Transport Modulation of Endothelial Cell Metabolism, *Biotechnology and Bioengineering*, 1991, 38(6), 588–602.

- [25] Shyy, Y.J., Hsieh, H.J., Usami, S., and Chien, S., Fluid Shear Stress Induces a Biphasic Response of Human Monocyte Chemotactic Protein 1 Gene Expression in Vascular Endothelium, *Proceedings of the National Academy of Sciences of the United States of America*, 1994, 91(11), 4678–4682.
- [26] Ye, T., Bull, J.L., Microbubble Expansion in a Flexible Tube, *ASME Journal of Biomechanical Engineering*, 2006, 128(4), 554–563.
- [27] Eshpuniyani, B., Bull, J.L., A Boundary Element Model of Vascular Gas Bubble Sticking and Sliding, in: Brebbia, C.A., ed, *Modeling in Medicine and Biology*, WIT Press, Southampton, 2005.
- [28] Eshpuniyani, B., Fowlkes, J.B., and Bull, J.L, A Boundary Element Model of Microbubble Sticking and Sliding in the Microcirculation, *International Journal of Heat and Mass Transfer*, 2008, 51(23–24), 5700–5711.
- [29] Pozrikidis, C., Numerical Simulation of Cell Motion in Tube Flow, *Annals of Biomedical Engineering*, 2004, 33(2), 165–178.
- [30] Greenspan, H.P., On the Motion of a Small Viscous Droplet That Wets a Surface, *Journal of Fluid Mechanics*, 1978, 84(1), 125–143.
- [31] Brebbia, C.A., *Boundary Elements: An Introductory Course*, WIT Press, UK, 1992.
- [32] Pozrikidis, C., *Boundary Integral and Singularity Methods for Linearized Viscous Flow*, Cambridge University Press, United States of America, 1992.